


Allele-specific alternative splicing of *Drosophila* Ribosomal protein S21 suppresses a lethal mutation in the Phosphorylated adaptor for RNA export (Phax) gene

Eric L. Garcia  ^{1,2,3,4,*}

¹Department of Microbiology, Immunology and Molecular Genetics, University of Kentucky College of Medicine, Lexington, KY 40536, USA,

²Department of Biology, University of Kentucky, Lexington, KY 40506, USA,

³Integrative Program for Biological and Genome Sciences, University of North Carolina at Chapel Hill, Chapel Hill, NC 27599, USA

⁴Present address: 675 Rose St., 300 TH Morgan Bldg., Lexington, KY 40506, USA.

*Corresponding author: Integrative Program for Biological and Genome Sciences, University of North Carolina at Chapel Hill, Chapel Hill, NC 27599, USA.

Email: elgarcia@unc.edu

Abstract

Genetic disruptions to the biogenesis of spliceosomal small-nuclear ribonucleoproteins in *Drosophila* cause wide-spread alternative splicing changes, including changes to the splicing of pre-mRNA for Ribosomal protein S21 (RpS21). Using a transposon mutant for the *Phosphorylated adaptor for RNA export (Phax)* gene, we demonstrate that changes in the splicing of *RpS21* transcripts have a strong influence on the developmental progression of *Phax*^{SH/SH} mutants. Different alleles of the *Drosophila* *RpS21* gene are circulating in common laboratory strains and cell lines. These alleles exhibit differences in *RpS21* intron retention and splicing efficiency. Differences in the splicing of *RpS21* transcripts account for prior conflicting observations of the phenotypic severity of *Phax*^{SH/SH} mutant stocks. The alleles uncover a strong splicing enhancer in *RpS21* transcripts that can fully suppress the larval lethality and partially suppress the pupal lethality exhibited by *Phax*^{SH/SH} mutant lines. In the absence of the splicing enhancer, the splicing of *RpS21* transcripts can be modulated in *trans* by the SR-rich B52 splicing factor. As *Phax*^{SH/SH} mutants exhibit wide-spread splicing changes in transcripts for other genes, findings here establish the importance of a single alternative splicing event, *RpS21* splicing or intron retention, to the developmental progression of *Drosophila*.

Keywords: phosphorylated adaptor for RNA export protein; Phax; ribosome; ribosomal protein; ribosomal protein S21; RpS21; alternative splicing; alternative polyadenylation; mRNA processing; snRNP biogenesis; Spinal Muscular Atrophy; *oho23B*; splicing factor; *cis*-element; exonic splicing enhancer; B52; survival motor neuron

Introduction

Depletion of core splicing machinery leads to specific, nonrandom changes in alternative splicing and gene expression, including changes to ribosomal protein (RP) coding genes (Pleiss et al. 2007; Saltzman et al. 2011; Garcia et al. 2016). Conversely, targeted inhibition of the transcription of highly expressed RP coding genes liberates the “hungry” spliceosome and results in distinct changes to alternative splicing (Munding et al. 2013; Talkish et al. 2019). Similarly, disease-associated mutations in RP coding genes and corresponding reductions in ribosomes cause specific changes in gene expression and the translation of select transcripts (Horos et al. 2012; Khajuria et al. 2018). The specificity of responses to different perturbations in the overall gene expression program supports an interconnected regulatory network for the biogenesis and homeostatic regulation of the spliceosome and the ribosome that intersects in the RNA processing of RP pre-mRNA.

Our prior transcriptomic profile of small-nuclear ribonucleoprotein (snRNP) biogenesis mutants in *Drosophila* identified wide-spread alternative splicing changes in *Phosphorylated adaptor*

for RNA export (*Phax*) mutants and *Survival motor neuron (Smn)* mutants (Garcia et al. 2016). *Phax* functions as a small-nuclear RNA (snRNA)-specific adapter to export Sm-class snRNAs from the nucleus, and *Smn* functions to assemble exported snRNAs into snRNPs in the cytoplasm (Ohno et al. 2000; Ohno 2012; Matera and Wang 2014). Full loss of fly *Smn* function results in a recessive larval lethality in *Drosophila* (Chan et al. 2003; Rajendra et al. 2007; Chang et al. 2008). In contrast, lethality can be genetically separated from a disruptive P element insertion in the *Drosophila* *Phax* gene, an insertion previously classified as lethal (Oh et al. 2003; Kahsai et al. 2016). Our lab and others have observed adult flies that are homozygous for this P element insertion in the *Phax* gene (Kahsai et al. 2016). Nevertheless, both *Phax* and *Smn* mutants exhibit lower steady-state levels of Sm-class snRNAs and an overlapping set of alternative splicing changes that includes changes in RP pre-mRNA, including a large change in the alternative splicing of pre-mRNA for Ribosomal protein S21 (RpS21) (Garcia et al. 2016).

RpS21 is component of the small subunit of the ribosome with functions in translation initiation and ribosome biogenesis

Received: June 01, 2022. Accepted: July 27, 2022

© The Author(s) 2022. Published by Oxford University Press on behalf of Genetics Society of America.

This is an Open Access article distributed under the terms of the Creative Commons Attribution License (<https://creativecommons.org/licenses/by/4.0/>), which permits unrestricted reuse, distribution, and reproduction in any medium, provided the original work is properly cited.

(Török et al. 1999; Sato et al. 2003; Tabb-Massey et al. 2003; Black and Johnson 2022). In *Drosophila*, haploinsufficient Rps21 mutants exhibit the classic Minute phenotype of short and thin bristles, prolonged development, and impaired viability (Török et al. 1999; Marygold et al. 2007). Homozygous Rps21 mutants display an overgrowth of hematopoietic organs like the overgrowth observed with fly *stubarista* (*sta/RpSA/P40*) and *Ribosomal protein S6* (*RpS6*) mutants (Watson et al. 1992; Stewart and Denell 1993; Török et al. 1999). Reduced levels of the core snRNP protein Smd3 have also been linked to a similar extension of development and concomitant overgrowth of hematopoietic tissues (Schenkel et al. 2002). In the context of our identification of large changes in Rps21 alternative splicing in other snRNP biogenesis mutants, the similarity in phenotypes between Rps21 and Smd3 mutants suggests that changes in Rps21 alternative splicing may impact developmental progression and organismal viability.

Here, we identify alternative alleles of Rps21 that encode transcripts with dramatic differences in alternative splicing. The different alleles uncover sequences in Rps21 exon 4 that function to enhance the splicing of exon 3 to exon 4. Remarkably, the Rps21 allele with the splicing enhancer sequences was capable of suppressing the lethality of a *Phax* P element insertion mutant. Hence, findings here reveal a discrete genetic background difference that can account for prior conflicting observations of the viability of different fly stocks from this *Phax*^{SH/SH} mutant line. Importantly, in the background of wide-spread alternative splicing changes, restoration of a single splicing event in Rps21 was ultimately able to rescue the developmental progression of homozygous *Phax*^{SH/SH} mutant flies.

Materials and methods

Fly strains and husbandry

Stocks were maintained on cornmeal and agar at room temperature (25 ± 1°C) in half-pint bottles. For crosses, sorting and the isolation of larvae, stocks were cultured on molasses and agar at room temperature (23 ± 3°C) unless indicated otherwise. Stocks for wild-type Ore-R (Oregon-R-modENCODE) and the reference genome strain iso-1 (*y*[1]; *Gr22b*[1] *Gr22d*[1] *cn*[1] *CG33964*[R4.2] *bw*[1] *speck*[1]; *MstProx*[1] *GstD5*[1] *Rh6*[1]) were obtained directly from the Bloomington *Drosophila* Stock Center (BDSC). Stocks for Canton-S (*Can-S*) and *w*¹¹¹⁸ were obtained from D.A. Harrison. Recombination of the UAS:*Phax-mVenus* transgene into the mutant *P*{*lacW*} *Phax*^{SH0641} (Oh et al. 2003) was previously described (Garcia et al. 2016). Here, *Phax*^{SH/SH} refers to homozygous lines with the P element insertion in the *Phax* gene (*P*{*lacW*} *Phax*^{SH0641}). The *armadillo* (*arm*) promoter-GAL4 driver *P*{*GAL4-arm*. S}11 (Sanson et al. 1996) was maintained in the *Phax*^{SH/SH} background.

To generate *Phax*^{SH/SH} mutant flies that were heterozygous and homozygous for the different Rps21 alleles, we crossed virgin female flies with a second chromosome balancer (*Cyo*; *Actin-GFP*), the Rps21^S short allele, and the P element insertion in the *Phax* gene to Canton-S wild-type male flies, homozygous for the Rps21^L long allele, described below. Meiotic recombination was allowed to take place in noncurly virgin female progeny from this initial cross. These virgin females were crossed to curly male progeny with the Rps21^L allele and the *Cyo*; *Actin-GFP* balancer. Progeny from this cross were genotyped to select a balanced recombinant with the Rps21^L long allele and the P element in the *Phax* gene, using a proteinase K (New England Biolabs Inc) method for the nonlethal isolation of DNA from *Drosophila* wings (Carvalho et al. 2009). Separate crosses were set up with balanced flies, containing the P element insertion in the *Phax* gene and different combinations of the Rps21^L long and Rps21^S

short allele. Through genotyping of unbalanced larvae, we isolated 3 separate stocks for each of the following genotypes: *Phax*^{SH/SH}, Rps21^{L/L}; *Phax*^{SH/SH}, Rps21^{S/L}; and *Phax*^{SH/SH}, Rps21^{S/S}.

For viability experiments, larvae were sorted on molasses-agar plates and transferred to cornmeal-agar vials. We sorted an average number (*n*) of 76 larvae for each replicate of the 23°C GAL4:UAS viability experiment, 100 larvae for the 27°C GAL4:UAS study, and 30 larvae for the viability study with homozygous or heterozygous Rps21 alleles in the *Phax*^{SH/SH} mutant background. A Student's t-test was used to calculate P-values.

Genotyping

DNA from whole animals or cells was isolated for genotyping with a Quick-DNA Tissue/Insect Miniprep Kit (Zymo Research) and a 4-place Mini Bead Mill Homogenizer (VWR) according to the manufacturer's protocol. Oligonucleotides used for PCR with Apex Taq Red (Genesee Sci) of the long allele or the short allele are listed in Supplementary Table 1. Gene-flanking oligonucleotides were used to clone the Rps21 gene from Oregon-R flies, S2-DRSC cells, and Kc167 cells into the *HindIII* and *BamHI* sites of pBlueScript II SK+ (Agilent) for sequencing with M13 forward and reverse primers. To genotype the *Phax*^{SH/SH} mutant, we used 2 sets of oligonucleotides. We used primers complementary to the *Phax* gene that flanked the P element insertion, and we used a P element out primer, an M13 sequencing primer, with a primer complementary to the 3'-end of the *Phax* gene. This oligonucleotide set confirmed the inverse directionality of the P element in relationship to the forward direction of the *Phax* gene. For primer design, gene and intergenic sequences were derived from Flybase and compatible with the current release FB2022_02 <http://flybase.org/> (Larkin et al. 2021).

Splicing mini-gene reporter design

Different wild-type and mutant Rps21 gene sequences, surrounding intron 3, were subcloned into the *KpnI* and *BamHI* sites in *pAc5.1B-EGFP* (Addgene plasmid # 21181; Elisa Izaurralde depositor). Wild-type and mutant gene sequences were generated as double-stranded DNA gene fragments (IDT gBlocks). Sequences for the minimal splicing reporter corresponded to the Rps21 gene from nucleotide 400 to nucleotide 611, based on the iso-1 reference sequence. These Rps21 gene sequences spanned the third intron from exon 3, 104 nucleotides upstream of the 5'-splice site, to immediately downstream of the AATAAA polyadenylation signal in exon 4, 50 nucleotides downstream of the intron 3 3'-splice site.

Cellfectin II Reagent (Gibco) was used for transfections of S2-DRSC according to the manufacturer's protocol. RNA was isolated on day 3 post transfection. RT-PCR was performed as indicated below with mini-gene specific primers (Supplementary Table 1). PCR products were separated on an agarose gel, stained with GelRed (Biotium), and imaged on a Gel Doc Ez (BIO-RAD). Bands were quantified with Image Lab 6.0.1 software (BIO-RAD). Percent Spliced In (PSI) was quantified as the percentage of spliced over total transcripts, and P-values were determined with a Student's t-test.

Cell culture and RNA interference

Drosophila S2-DRSC (DGRC Stock 181; <https://dgrc.bio.indiana.edu/stock/181>; RRID: CVCL_Z992) and Kc167 (DGRC Stock 1; <https://dgrc.bio.indiana.edu/stock/1>; RRID: CVCL_Z834) cells were acquired directly from the *Drosophila* Genomics Resource Center (DGRC) (Schneider 1972; Cherbas et al. 1988). Both cell

lines were cultured in Schneider's *Drosophila* Medium supplemented with 10% fetal bovine serum and 1× penicillin–streptomycin–glutamine (Gibco). RNA from S2-DRSC cells was used for reverse transcription with Superscript III (Invitrogen) to make cDNA. This cDNA and Apex Taq Red (Genesee Sci) were used with T7 promoter–fusion primers (Supplementary Table 1) to amplify B52. Sequences for T7–fusion primers were derived from cell-screening “R” and “S” primer sets from the *Drosophila* RNAi Screening Center (DRSC) (Hu et al. 2020). PCR products served as templates for the overnight *in vitro* transcription with MEGAscript (Invitrogen) to generate double-stranded RNA for RNA interference (RNAi). Approximately 15 μg of dsRNA was added to each sample in a separate well of a 6-well tissue culture dish. The dsRNA was added on the first, third, and fifth days of the treatment. Samples were taken for RNA isolation on day 6.

HeLa and HepG2 cell pellets were generously supplied by the labs of K.A. Fields and B.T. Spear, respectively. Human cell pellets were immediately put in TRIzol reagent (Invitrogen) and RNA isolated for RT-PCR with human RPS21e-specific primers, as indicated below.

Western blotting

Protein was isolated from wild-type and sorted larvae approximately 4 days post-egg laying. Protein was isolated by crushing larvae in 1× RIPA Buffer (Thermo Scientific) supplemented with Halt Protease (Thermo Scientific) and Halt Phosphatase (Thermo Scientific) inhibitor cocktails. Lysates were precipitated with trichloroacetic acid, washed with methanol, and dried (80°C for 10 min) before resuspension in 1× Sample Loading Buffer (LI-COR). Protein samples were separated on NuPAGE 4–12% Bis–Tris gels in 1× NuPAGE MES SDS running buffer. Separated proteins were transferred to 0.2-μm low fluorescence PVDF (Thermo Scientific) and blocked with Odyssey Blocking Buffer (TBS) (LI-COR). A rabbit polyclonal antibody was generated to an antigen for the protein product of CG33057 by ABclonal. A CG33057 gene fragment (amino acids 1–212) was subcloned into the pGEX-4T-AB1 vector for protein expression and purification. Primary antibodies for CG33057, RpS21 (Abcam # ab90874), and RpS6 (C.896.4) (Invitrogen) were used here at a 1:2,000 concentration. The monoclonal antibody to α-tubulin (4A1-s) developed by M.T. Fuller at Stanford University was obtained from the Developmental Studies Hybridoma Bank, created by the NICHD of the NIH and maintained at The University of Iowa, Department of Biology, Iowa City, IA, USA. The α-tubulin antibody was used at a 1:30,000 concentration. LI-COR infrared IR dye-conjugated anti-mouse and -rabbit secondaries were used at a 1:15,000 concentration to image and quantify proteins with an Odyssey Imager (LI-COR) and Image Studio Lite software (LI-COR). For statistical analysis, P-values were determined with a Student's t-test.

RNA isolation, RT-PCR, and real-time PCR

RNA was isolated from crushed larvae approximately 4 days post-egg laying. RNA was isolated with TRIzol reagent according to the manufacturer's protocol. Isolated RNA was subjected to an additional round of DNase with TURBO DNase (Invitrogen), followed by phenol chloroform extraction. Reverse transcription (RT) was performed with Superscript III (Invitrogen) and random hexamers. PCR was performed with Apex Taq Red (Genesee Sci), and limited cycles of amplification with intron flanking oligos. PCR products were separated on an agarose gel in 1× TBE, stained with GelRed (Biotium), and imaged on a Gel Doc Ez (BIO-RAD). Separated bands were quantified on unaltered images with Image Lab 6.0.1 software (BIO-RAD). PSI was quantified as

indicated above, as the percentage of spliced over total transcripts. For statistical analysis, P-values were determined with a Student's t-test. Real-time PCRs of cDNA were conducted on a StepOnePlus System (Applied Biosystems), using Maxima (Thermo Scientific) or PowerUp (Applied Biosystems) SYBR Green/ROX master mixes. Three biological replicates were tested for each genotype. The ΔΔCt method was used to quantify differences, and P-values were determined with a Student's t-test. Gene-specific primer sequences are listed in Supplementary Table 1.

RNA-seq analyses

RNA-seq analysis was performed on original fastq files that were previously deposited in the NCBI Gene Expression Omnibus (GEO) (Edgar et al. 2002). Files are indicated below. Transcript abundance was quantified with kallisto (Bray et al. 2016) and differential analysis was performed with sleuth (Pimentel et al. 2017). HISAT2 (Kim et al. 2019) and Samtools (Danecek et al. 2021) were used to align RNA-seq reads to Release 6 of the *Drosophila melanogaster* genome (Hoskins et al. 2015) for visualization and Sashimi plot comparison with the Integrative Genomics Viewer (Robinson et al. 2011, 2017).

Results

RNA-seq uncovered an increase in RpS21 intron 3 retention in fly *Phax*^{SH/SH} mutants

Prior transcriptome analysis uncovered an overlapping set of alternative splicing changes in *Drosophila* snRNP biogenesis mutants. Notably, *Phax* and *Smn* mutants exhibited a large change in alternative splicing across intron 3 of the Ribosomal protein S21 (RpS21) gene (Garcia et al. 2016). As shown here in RNA-seq data from *Phax*^{SH/SH} mutants, a disruption of snRNA nuclear export and snRNP biogenesis leads to a large increase in intron 3 retention in RpS21 transcripts, and a parallel decrease in reads spanning the RpS21 exon 3 and 4 splice junction surrounding intron 3 (Fig. 1, a and b) (Garcia et al. 2016). These changes were uncovered previously in global alternative splicing analysis (Garcia et al. 2016) and in transcript-specific analysis here (Fig. 1c and Supplementary Table 2). *Phax*^{SH/SH} mutants display an increase in transcripts for the RpS21-RE isoform that retains intron 3, and a corresponding decrease in RpS21-RA and -RF isoforms, which splice out intron 3 (Fig. 1c). The phenotypic consequences of these changes in RpS21 intron retention are unknown.

The splicing pattern of the predominant terminal exon of RpS21 is highly conserved from flies to humans

Splicing of the third intron of RpS21 pre-mRNA modulates the carboxy-terminus of the encoded RpS21 protein (Fig. 2a). The last 3 amino acids at the carboxy-terminus of the RpS21 protein are lysine (K), asparagine (N), and phenylalanine (F). The splice junction between exons 3 and 4 spans the K codon. The 3 carboxy-terminal amino acids of fly RpS21 are conserved with the human RPS21e protein, and, most notably, the human RPS21e transcripts also include a splice junction that spans the terminal K codon (Fig. 2a). In unspliced RpS21 transcripts, the intron contains the third wobble base of the terminal K codon and a following stop codon. The same pattern is conserved in the corresponding intron of human RPS21e transcripts. Human cell lines also show evidence of retention of the corresponding intron of RPS21e (Fig. 2b). Hence, this is an exceptionally well-conserved splicing pattern from flies to humans.

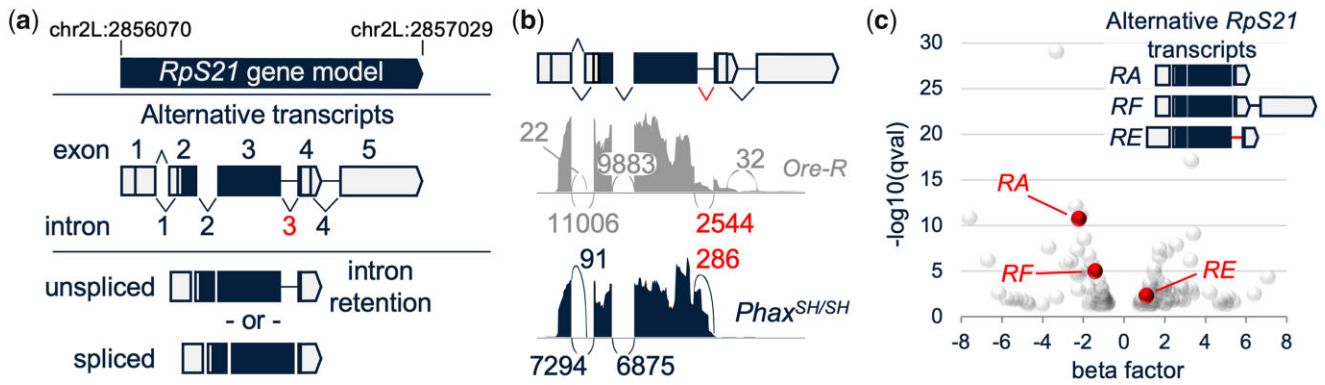


Fig. 1. RNA-seq evidence for the alternative splicing of *RpS21* transcripts in *Phax^{SH/SH}* mutants. a) *RpS21* gene model that includes constitutive and alternative splicing patterns of *RpS21*. Top: *Drosophila RpS21* gene model on chromosome 2L (chr2L); middle: alternative *RpS21* transcripts with numbered exons and introns. Splicing across intron 1 includes alternative 3'-splice sites. Splicing across intron 2 is constitutive. Introns 3 and 4 are alternatively spliced or retained. The right-side angled points of the boxes for exons 4 and 5 indicate sites of alternative polyadenylation. Exon 1 includes alternative transcription start sites. Bottom: transcripts with the conserved intron 3 retention (unspliced) or alternatively spliced exon 3 to exon 4 (spliced). Note, the vast majority of *RpS21* transcripts in the whole animals and the cell lines tested here utilize the proximal polyadenylation signal in exon 4. b) A sashimi plot graph of exon junction reads derived from RNA-seq of wild-type *Oregon-R (Ore-R)* and *Phax^{SH/SH}* mutant (*Phax^{SH/SH}*) animals. Curved lines indicate the locations of junction reads that span the relative locations indicated in the alternative *RpS21* transcript model at the top. The numbers indicate the total number of reads spanning those specific exon junctions. Reads spanning the exon 3 to exon 4 junction are indicated in red. c) Volcano plot of transcript differences between wild-type *Oregon-R* and *Phax^{SH/SH}* mutant animals. Transcripts with higher levels in the *Phax^{SH/SH}* mutants are on the right, and transcripts with lower levels are on the left. The y-axis is a negative log base 10 of the *q*-value, which is a false discovery rate (FDR) adjusted *p*-value (FDR < 0.05). The x-axis is a beta factor, an approximation of a normalized fold change, using the Wald test of the sleuth R package. Alternative differentially expressed *RpS21* transcripts are indicated in red.

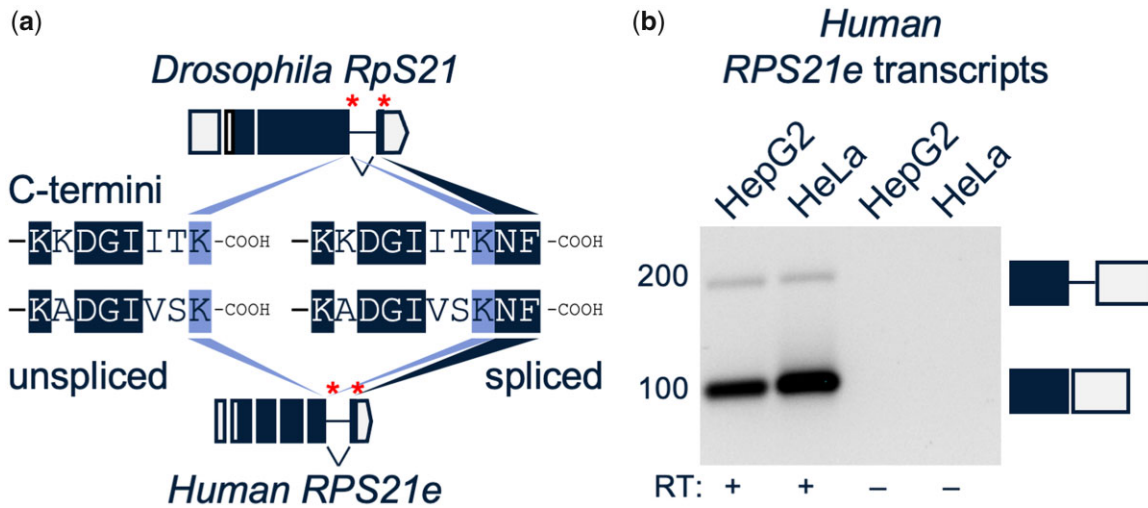


Fig. 2. Conserved features of the terminal *RpS21* splice junction that overlaps the protein coding sequences. a) Transcript models of fly *RpS21* top and human *RPS21e* bottom. Alternative stop codons are indicated with asterisks. Middle: alternative carboxy-terminal (C-termini) ends encoded by unspliced and spliced transcripts. Identical amino acids are shaded, and the conserved terminal lysine (K) is shaded separately. b) Intron retention of human *RPS21e* transcripts. Image of a GelRed-stained agarose gel of RT-PCR products, amplified with primers that flank the terminal exon junction of human *RPS21e* transcripts. Image was converted to grayscale, inverted, and contrast adjusted. Right: boxes depict the mobility of PCR products corresponding to unspliced (top) and spliced (bottom) transcripts.

Phax^{SH/SH} mutants exhibit an expected decline in viability but a surprising lack of any adult escapers

As this conserved splicing event in *RpS21* transcripts was altered in *Phax^{SH/SH}* mutant flies, *Phax^{SH/SH}* mutants and a *UAS-Phax* rescue transgene were used to determine how changes in this splicing event might contribute to organismal viability. In agreement with our previous findings (Garcia et al. 2016), the *Phax^{SH/SH}* mutants exhibited a large decrease in viability, as compared to wild-type *Oregon-R* controls (Supplementary Fig. 1a). Also, as before (Garcia et al. 2016), this decrease in viability was partially rescued by the ubiquitous expression of a wild-type *UAS-Phax*

transgene with an *armadillo-GAL4* driver (Supplementary Fig. 1a). However, unlike the previous study, ubiquitous expression of the *UAS-Phax* transgene did not lead to the eclosion of any adult flies (Supplementary Fig. 1a). In our previous study, approximately 30% of *Phax*-transgene expressing larvae developed to adulthood (Garcia et al. 2016). As the yeast-derived *GAL4-UAS* system is optimal at approximately 27°C, we also assayed viability at 27°C. Temperature did not account for the discrepancies between our current and prior viability studies, as viability at 27°C was roughly equivalent to the viability at 23°C (Supplementary Fig. 1, a and b). Prior to our rescue experiments and the site-specific integration of the *UAS-Phax* transgene into the *Phax^{SH/SH}* mutant

background, adult escapers, homozygous for the P element insertion in the *Phax* gene, were intermittently detectable in different stocks of this *Phax^{SH/SH}* mutant line (Oh et al. 2003; Kahsai et al. 2016; Garcia et al. 2016). We hypothesized that subtle genetic background differences might contribute to the observed differences in the viability of different stocks of the *Phax^{SH/SH}* mutant and in our transgenic rescue experiments.

Proper splicing across intron 3 of *RpS21* is linked to *Phax* expression

Changes in *RpS21* intron 3 retention parallel the observed changes in viability of *Phax^{SH/SH}* mutant and rescue animals. The splicing across *RpS21* intron 3 is normally inefficient, as wild-type *Oregon-R* larvae exhibit a high baseline level of intron 3 retention (Fig. 3a). In *Oregon-R* animals, the percentage of fully spliced *RpS21* transcripts across intron 3 averaged a low 56 PSI (Fig. 3b). Splicing across intron 3 was worse in the *Phax^{SH/SH}* mutants, evident as a visible increase in the ratio of unspliced to spliced transcripts (Fig. 3a) and a decrease in the percentage of fully spliced transcripts to 34 PSI (Fig. 3b). These changes in *RpS21* splicing were fully rescued by ubiquitous expression of the *UAS-Phax* transgene (Fig. 3, a and b). Nevertheless, the rescue of *RpS21* alternative splicing did not fully restore the developmental progression in *UAS-Phax* expressing animals.

Phax^{SH/SH} mutant changes in alternative splicing affect the steady-state levels of encoded proteins

Anticipated changes in steady-state protein levels accompanied the changes in alternative splicing in the *Phax^{SH/SH}* mutants. *Phax^{SH/SH}* mutants exhibited a decrease in steady-state levels of *RpS21* protein relative to a tubulin loading control (Fig. 3, c and d). Levels of *RpS21* protein were rescued by expression of the *UAS-Phax* transgene (Fig. 3, c and d). Protein levels of another small subunit protein, ribosomal protein S6 (*RpS6*), were also down in the *Phax^{SH/SH}* mutants (Fig. 3, c and d). Although small changes in *RpS6* transcripts were found in our transcript-specific analysis here, changes in *RpS6* alternative splicing were not uncovered in our more stringent prior analysis (Garcia et al. 2016). Hence, changes in *RpS6* protein levels could reflect the more dramatic changes in *RpS21* alternative splicing or broader splicing disruptions exhibited by the *Phax^{SH/SH}* mutants. As an additional control for anticipated protein level changes, we blotted for the protein product of the computed gene CG33057, which encodes an ortholog of the yeast tRNA 2'-phosphotransferase protein (TPT1). Transcripts for CG33057 are contained entirely within an intron of transcripts for the *monkey king protein (mkg-p)* gene that is retained in snRNP biogenesis mutants (Garcia et al. 2016). We detected an increase in levels of a protein of the expected molecular weight for the fly TPT1 ortholog in lysates from *Phax^{SH/SH}* mutants (Fig. 3c). Protein levels of the putative fly TPT1 ortholog

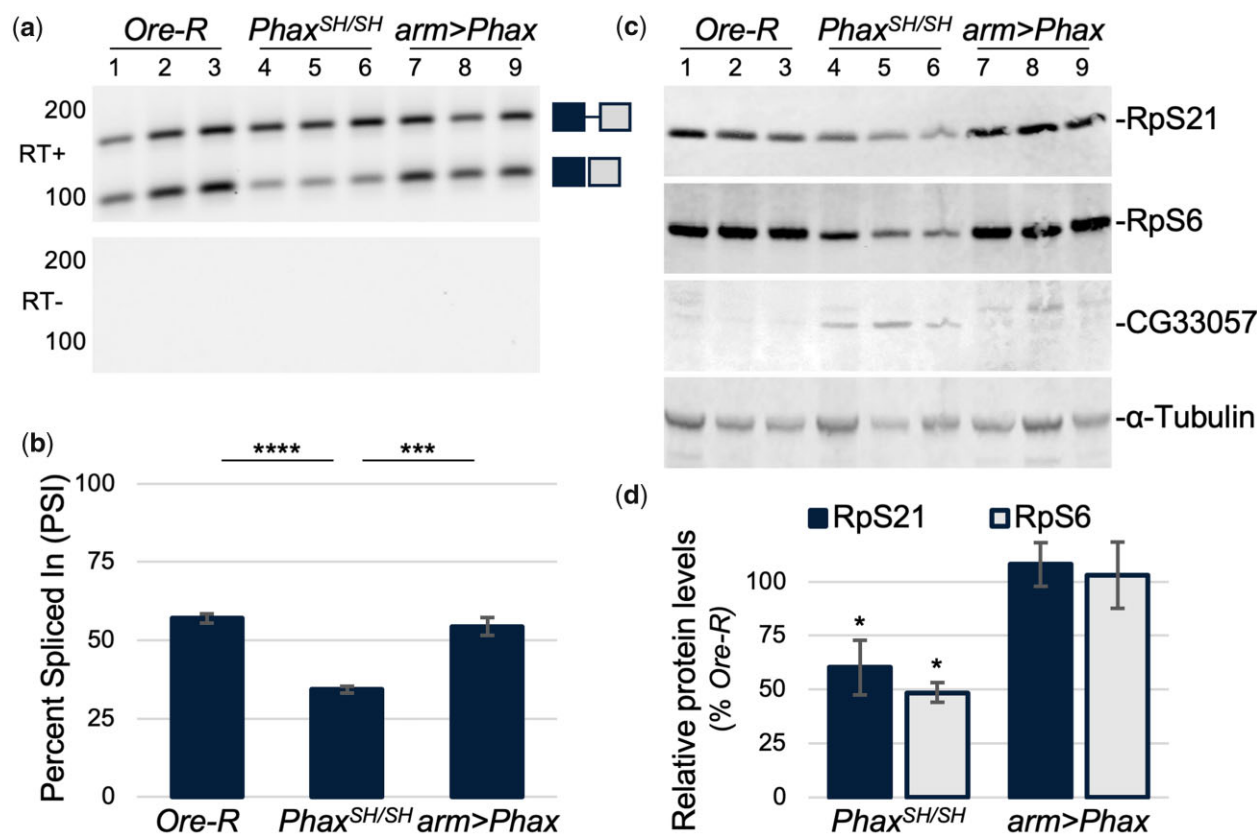


Fig. 3. Differential abundance of *RpS21* transcripts and *RpS21* protein levels in *Phax^{SH/SH}* mutant and rescue animals. a) Increase in *RpS21* intron 3 retention in *Phax^{SH/SH}* mutants and corresponding decrease upon expression of the *Phax* transgene. Transgenic rescue animals (*arm>Phax*) utilized an *armadillo-GAL4* driver (*arm*) and a *UAS:Phax-mVenus* transgene (*Phax*) in the *Phax^{SH/SH}* mutant background. Image of a GelRed-stained agarose gel of RT-PCR products, amplified with primers flanking the predominant terminal exon junction, encompassing intron 3 of *Drosophila RpS21* transcripts. Gels include PCR products or negative controls from reactions with (RT+) or without reverse transcriptase (RT-), respectively. Gel image was adjusted as in Fig. 2b. Of note, *RpS21* terminal intron 4 from Fig. 1a is rarely spliced out of *RpS21* transcripts that utilize the distal polyadenylation signal. *RpS21* distal polyadenylated transcripts are also relatively low compared to proximal polyadenylated transcripts in the whole animals and cells used here. b) Quantification of the percentage of splicing from exon 3 to exon 4 in (a). The graph is the percentage of spliced to total transcripts, shown as PSI. c) Western blots for the indicated proteins. d) Quantification of the *RpS21* and *RpS6* protein levels relative to α -tubulin from (c). Relative levels of these proteins in *Oregon-R* were set to 100%. *P < 0.05; ***P < 0.001; and ****P < 0.0001.

returned to baseline levels upon expression of the *UAS-Phax* transgene (Fig. 3c). However, like the noted changes in *RpS21* alternative splicing, rescue of protein levels was not sufficient to restore the developmental progression of *UAS-Phax* transgene expressing animals.

Common *Drosophila* flies and cell lines have different alleles of the *RpS21* gene

DNA sequencing revealed a surprising allelic heterogeneity in exon 4 of *RpS21*, immediately downstream of intron 3, in common laboratory flies and cell lines. Using *RpS21* gene-flanking primers, we subcloned and sequenced the *RpS21* gene in *Oregon-R* flies, S2-DRSC cells, and Kc167 cells. Surprisingly, *RpS21* exon 4 from S2-DRSC cells and *Oregon-R* flies contained a 7-nucleotide deletion and an additional adenine to thymine transversion relative to Kc167 cells and the *Drosophila* genome reference strain iso-1 (Fig. 4a). Available genome assemblies also support the identified allelic heterogeneity in *RpS21* exon 4 amongst different *Drosophila* cell lines (Supplementary Fig. 2). This subtle genetic difference was used to design allele-specific primers to genotype additional fly lines. The *Phax*^{SH/SH} mutants, *Armado*-GAL4 rescue line (*arm*), and the widely used *w*¹¹¹⁸ mutant contained the short (S) *RpS21*^S allele found in *Oregon-R* flies and S2-DRSC cells (Fig. 4b). The alternative wild-type *Canton-S* flies had the long (L) *RpS21*^L allele like iso-1 flies and Kc167 cells (Fig. 4b). The genetic difference in exon 4 overlapped a predicted Exonic Splicing Enhancer (ESE) in the longer *RpS21*^L allele (Cartegni et al. 2003). Therefore, we hypothesized that the discrete genetic differences in exon 4 could affect the splicing across intron 3 of *RpS21* pre-mRNA.

Allelic differences in the *RpS21* gene correspond to differences in the splicing of *RpS21* transcripts

Indeed, the genetic differences in exon 4 correlated with the expected differences in intron 3 retention in *RpS21* transcripts (Fig. 4, c and d). *RpS21* transcripts from *Oregon-R* and *w*¹¹¹⁸ flies exhibited a high level of intron 3 retention and a relatively low, approximately 60 PSI, level of spliced transcripts. In contrast, *Canton-S* and iso-1 flies with the longer *RpS21* allele, containing the predicted ESE, had little to no intron 3 retention and a high, greater than 99 PSI, level of spliced transcripts (Fig. 4c). This pattern was also evident in *Drosophila* Kc167 cells with the long *RpS21* allele vs. S2-DRSC cells, lacking the putative ESE (Fig. 4, d and e). Kc167 cells exhibited greater than 99 PSI with no *RpS21* intron 3 retention, and S2-DRSC cells had a high level of intron 3 retention and a low, 55 PSI, level of spliced transcripts (Fig. 4, d and e). The increased splicing efficiency of *RpS21* transcripts from the longer allele supports the prediction that the additional GC-rich sequences in exon 4 function as a strong ESE.

Predicted ESE sequences in exon 4 of *RpS21* transcripts enhance the splicing of exon 3 to exon 4

We constructed an *RpS21* mini-gene splicing reporter to further test the prediction that the additional sequences in exon 4 of the long *RpS21* allele function as an ESE. The minimal *RpS21* mini-gene spanned the 3'-end of exon 3 to the end of exon 4 with (*miniS21*^L) and without (*miniS21*^S) the putative ESE in exon 4 (Supplementary Fig. 3a). The splicing reporter utilized a heterologous *Actin5C* promoter and an SV40 polyadenylation signal (Supplementary Fig. 3a). We created an additional mini-gene without the predicted ESE sequences that contains a consensus 5'-splice site (*miniS21*^S A>G) (Supplementary Fig. 3a). The A>G

mutation was designed to test the potential contribution of the unpaired A nucleotide in the 5'-spliced site to *RpS21* intron 3 retention. As expected, the PSI of the *miniS21*^S A>G reporter was significantly higher than the *miniS21*^S reporter with the endogenous 5'-splice site, supporting a small contribution of this seemingly weak 5'-splice site to *RpS21* intron 3 retention. However, the splicing efficiency of all 3 mini-gene reporters was greater than 80 PSI, which exceeded the inefficient splicing of endogenous transcripts from the *RpS21* short allele (Supplementary Fig. 3, b and c). This suggests that additional sequences that were not included in the mini-gene splicing reporter likely contribute to the high level of *RpS21* intron 3 retention in transcripts encoded by the short allele. Nevertheless, the *RpS21* mini-gene with the putative ESE in exon 4 (*miniS21*^L) produced transcripts with significantly less intron retention and a greater PSI than transcripts from either mini-gene lacking the ESE sequences, which further supports the hypothesis that the additional nucleotides in the long allele function to enhance the splicing of *RpS21* exon 3 to exon 4 (Supplementary Fig. 3, b and c).

Knockdown of the B52 splicing factor decreases *RpS21* intron 3 retention in *RpS21* transcripts without the predicted ESE in exon 4

A prior cross-comparison of published RNA-seq data for local splicing variations revealed a decrease in *RpS21* intron 3 retention upon RNAi knockdown of mRNA for the splicing factor B52 in *Drosophila* S2 cells (Srivastava et al. 2021). As expected from these transcriptomic findings, B52 knockdown in S2-DRSC cells here led to a decrease in *RpS21* intron 3 retention and a corresponding 30% increase in the percentage of spliced *RpS21* transcripts (Fig. 5, a–c). However, B52 knockdown in Kc167 cells did not appear to affect the splicing across intron 3 of *RpS21* in those cells, as the splicing efficiency of *RpS21* in Kc167 cells without B52 knockdown is already very high (>99 PSI) (Fig. 5, a–c). In other words, the long allele of *RpS21*, with the predicted ESE in exon 4, appears to short circuit or counter the inhibitory regulation of pre-mRNA splicing of *RpS21* exon 3 to exon 4 by B52.

The *RpS21* ESE-containing allele suppresses the pupal lethality of the *Phax*^{SH/SH} mutants

With mounting evidence for the high splicing efficiency of the long *RpS21* allele, we asked whether this allele could restore the developmental progression of snRNP biogenesis mutants. Notably, the long allele of *RpS21* was able to partially restore the developmental progression of *Phax*^{SH/SH} mutants (Fig. 6, a and b). At the pupal stage, the presence of the long *RpS21* allele (*RpS21*^L) significantly improved the viability of *Phax*^{SH/SH} mutants in an allele dose dependent manner (Fig. 6a). Furthermore, unlike *Phax*^{SH/SH} mutants with only the short *RpS21* allele (*RpS21*^{S/S}), *Phax*^{SH/SH} mutants that were either heterozygous for *RpS21* (*RpS21*^{S/L}) or homozygous for the long allele (*RpS21*^{L/L}) produced adult escapers (Fig. 6b). To date, no progenies have been observed from any of the adult *Phax* escapers. Nevertheless, we conclude that different *RpS21* alleles likely account for our prior observations of intermittent adult escapers in *Phax*^{SH/SH} mutant stocks.

The *RpS21* ESE-containing allele decreases *RpS21* intron 3 retention in the *Phax*^{SH/SH} mutants in an allele dose dependent manner

In the *Phax*^{SH/SH} mutant background, the presence of the long *RpS21*^L allele rescues the splicing of exon 3 to exon 4 of *RpS21* transcripts (Fig. 6c). *Phax*^{SH/SH} mutant larvae that are homozygous for the short *RpS21*^S allele (*RpS21*^{S/S}) exhibited the highest

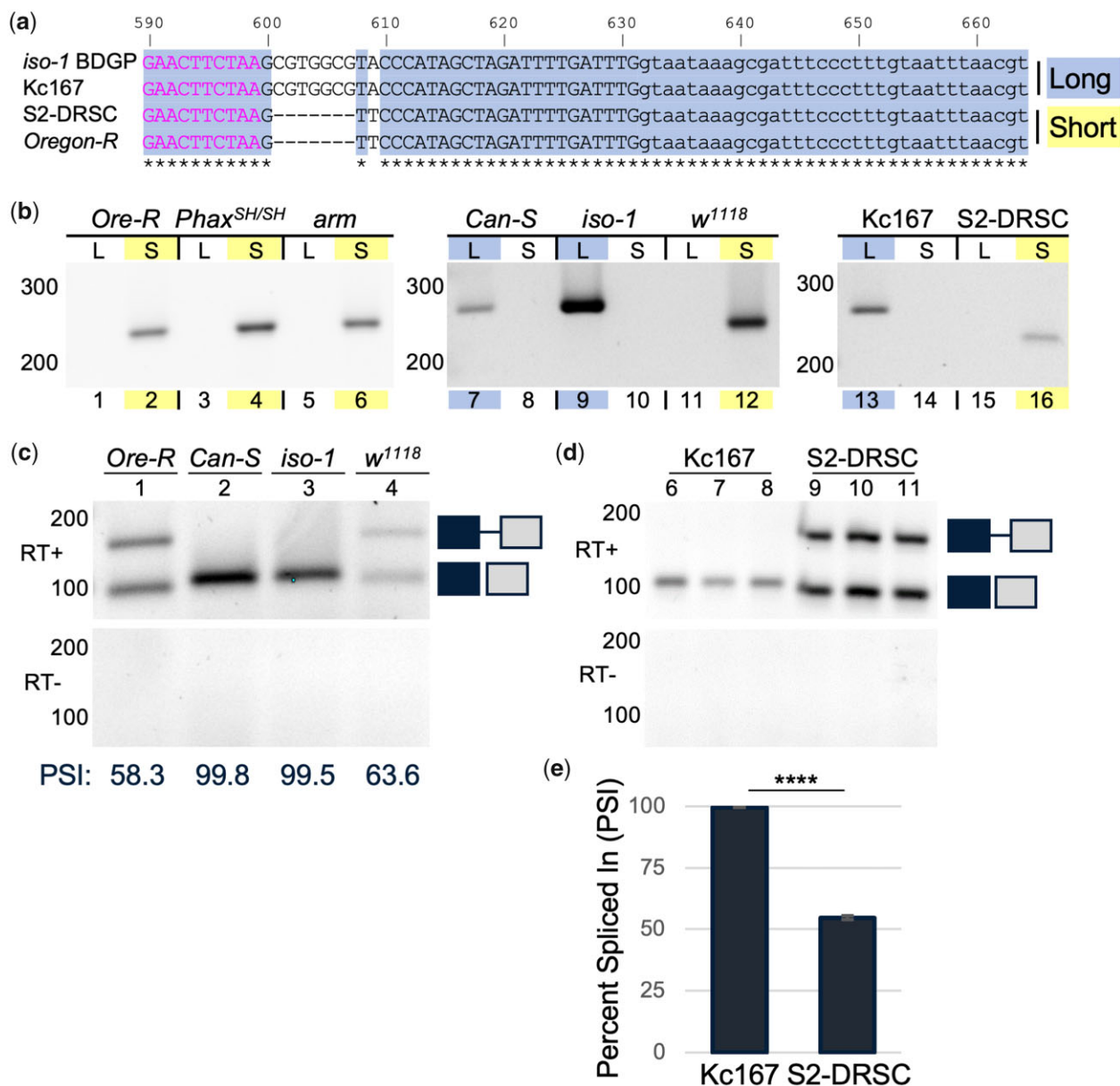


Fig. 4. Alternate Rps21 alleles and corresponding differences in transcript abundance. a) Multiple sequence alignment of the predominant exon 4 of Rps21. Subcloned and sequenced DNA from Kc167 and S2-DRSC cell lines and Oregon-R flies was aligned to the *Drosophila* genome reference strain (iso-1). Identical bases are shaded in blue with an asterisk below. C-terminal coding sequences are indicated on the left in pink. Descriptors for the long allele (L) top and short allele (S) bottom are also shaded to coincide with the genotyping in (b), where allele-specific primers were used to amplify DNA from the indicated flies and cells. GelRed-stained agarose gels of PCR products were adjusted as in Fig. 2b. c) Relative abundance of Rps21 transcripts in the indicated fly lines. Inverted GelRed-stained agarose gels of RT-PCR products, as indicated previously. Quantification of the blot in PSI is indicated below each lane. d) Relative abundance of Rps21 transcripts in Kc167 and S2-DRSC cells. Inverted GelRed-stained agarose gels of RT-PCR products, as indicated previously. e) Quantification of the PSI for transcripts from (d). **** $P < 0.0001$.

level of intron 3 retention and the lowest level of exon 3 and 4 splicing (21 PSI) relative to Oregon-R controls (Fig. 6, c and d) or larvae with even a single copy of the long Rps21^L allele (Fig. 6, c and d). Phax^{SH/SH} mutants, which are heterozygous for the Rps21 short and long alleles (Rps21^{S/L}), exhibited similar levels of intron 3 retention and splicing (58 PSI) as wild-type Oregon-R animals that are homozygous for the short allele (Rps21^{S/S}) (Figs. 6, c and d and 3, a and b). Phax^{SH/SH} mutants that are homozygous for the long Rps21^L allele (Rps21^{L/L}) have levels of intron 3 retention and splicing (98 PSI) that are like wild-type Canton-S animals (99 PSI)

with no genetic perturbations of snRNP biogenesis (Fig. 6, c and d). Hence, we conclude that the long Rps21^L allele is sufficient to rescue the perturbation of Rps21 splicing caused by P element mutations in the Phax gene.

Discussion

The alternative splicing of pre-mRNA for RPs has the potential to regulate the overall abundance and composition of ribosomes. Changes in either ribosome abundance or composition can cause

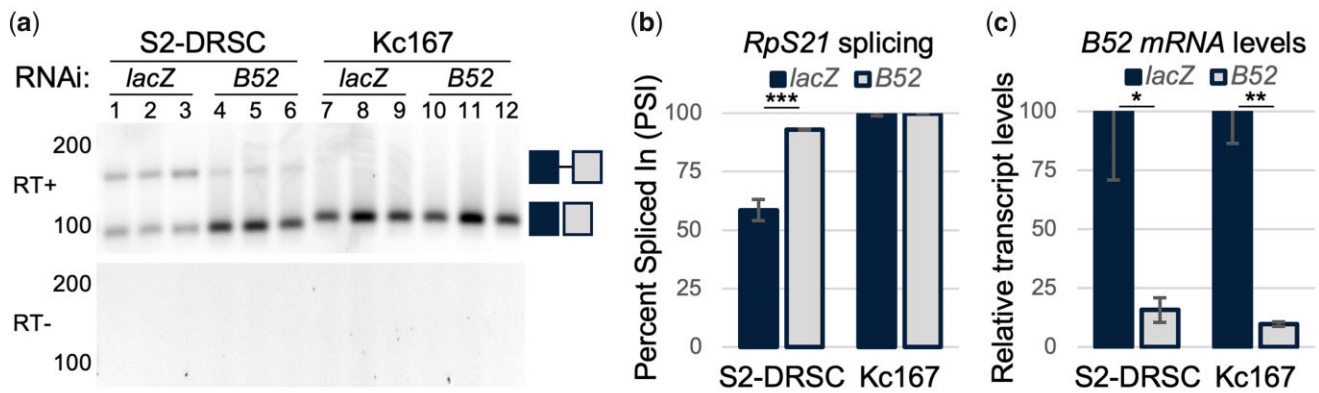


Fig. 5. RpS21 alternative splicing upon control or B52 RNAi depletion. a) RT-PCR of RpS21 in control (*lacZ*) and B52 depleted S2-DRSC and Kc167 cells. Images were inverted and contrast adjusted as indicated previously. b) Quantification of PSI of RpS21 transcripts from (a). c) Real-time qRT-PCR of B52 transcript levels relative to α -tubulin transcripts, determined by the $\Delta\Delta C_t$ method. * $P < 0.05$; ** $P < 0.01$; and *** $P < 0.001$.

specific changes to gene expression and affect the protein synthesis of select transcripts (Horos et al. 2012; Khajuria et al. 2018). Our prior transcriptome analysis of snRNP biogenesis mutants uncovered specific changes to the alternative splicing of RP pre-mRNA (Garcia et al. 2016). As shown here, the *Phax^{SH/SH}* mutant changes to RpS21 pre-mRNA correlated with a decrease in RpS21 and RpS6 protein abundance that is consistent with a putative decrease in ribosome numbers. In addition, RpS21 intron 3 retention encodes an RpS21 protein isoform that is 2 amino acids shorter at the carboxy-terminus. Thus, in addition to ribosome abundance, the modulation of the alternative splicing of RP pre-mRNA can subtly alter ribosome composition.

Disruptions to ribosome numbers have been previously linked to disease. Mutations in numerous RP coding genes, other than human RPS21e, are associated with the blood disorder Diamond-Blackfan anemia (DBA) (Narla and Ebert 2010; Horos et al. 2012; Mills and Green 2017; Khajuria et al. 2018; Aspesi and Ellis 2019; Costa et al. 2020). DBA-associated RP gene mutations have been linked to reductions in ribosome levels (Khajuria et al. 2018). A similar decrease in ribosome numbers has been observed in mouse models of the neuromuscular disease Spinal Muscular Atrophy (SMA) (Bernabò et al. 2017). SMA is caused by mutations in the human *Survival Motor Neuron 1* (SMN1) gene (Lefebvre et al. 1995). In addition to a reduction in axonal ribosomes, SMA model mice exhibited lower levels of Rps6 protein and a wide-spread decrease in the translation efficiency of RP transcripts, including transcripts for mouse Rps21 and Rps6 (Bernabò et al. 2017). The reductions of fly Rps21 and Rps6 proteins in the *Phax^{SH/SH}* mutants are consistent with the finding of disrupted ribosome homeostasis in SMA model mice. How specific alternative splicing events contribute to RP levels and overall ribosome numbers remains to be determined, but findings here suggest that missplicing of RP coding transcripts may contribute to the observed reduction in RP levels and possibly ribosome numbers. Importantly, however, the long ESE-containing Rps21 allele has, to date, been insufficient to suppress the larval lethality of fly *Smn* null mutants.

In the absence of the strong ESE in exon 4, Rps21 alternative splicing was negatively regulated in *trans* by the SR-rich B52 splicing factor. The human ESEfinder predicts a Serine and Arginine

Rich Splicing Factor 6 (SRSF6)-binding site, nucleotides –GGCGUA–, that overlaps the allelic difference in exon 4 of Rps21 transcripts from the longer Rps21^L allele (Fig. 4a) (Cartegni et al. 2003). To date, our RNAi screens have yet to identify an orthologous *Drosophila* splicing factor and/or component of the 3'-cleavage and polyadenylation machinery that binds to this putative ESE in exon 4 to enhance Rps21 splicing. The negative regulation of Rps21 splicing by B52, occurring in Rps21 transcripts without this ESE, likely requires additional cis-regulatory sequences beyond intron 3 and proximal sequences in the adjacent exons. The minimal Rps21 splicing reporter without the ESE had a notably high PSI (>80 PSI) relative to the low PSI (~58 PSI) of corresponding endogenous Rps21 transcripts. In addition to a heterologous promoter and polyadenylation signal, the minimal reporter included only intron 3, the short downstream exon 4, and a mere 100 out of 192 nucleotides of upstream exon 3. B52 has a demonstrated affinity for structured RNA with accessible single-stranded binding sites (Shi et al. 1997). Binding of B52 to Rps21 transcripts may therefore require additional upstream or downstream sequences necessary for proper RNA structure.

Overexpression of B52 has been linked to increased growth and depletion to decreased growth (Fernando et al. 2015; Wada et al. 2021). In addition to Rps21, third-party analysis of published RNA-seq data of B52 knockdowns in S2 cells uncovered alternative splicing of *yorkie* transcripts, a transcriptional co-activator in Hippo signaling (Srivastava et al. 2021). Hippo signaling is a highly conserved pathway that controls organ size (Halder and Johnson 2011; Hariharan 2015; Yu et al. 2015; Meng et al. 2016). Depletion of 1 copy of the *yorkie* gene enhanced the dysregulated cell-growth phenotype of heterozygous RP mutants (Wada et al. 2021). Through the concerted regulation of the alternative splicing of Rps21 and *yorkie* transcripts, splicing factors like B52 can synchronize the ribosome with cell growth signals.

Proteomic and phospho-proteomic studies of the human RPS21e protein have identified posttranslational modifications at the carboxy-terminus of the protein that are likely impacted by the alternative splicing of the terminal exon of RPS21e transcripts (Choudhary et al. 2009; Mertins et al. 2013, 2016; Akimov et al. 2018). Overall, our findings are consistent with a model for the regulation of Rps21 through the alternative splicing of the

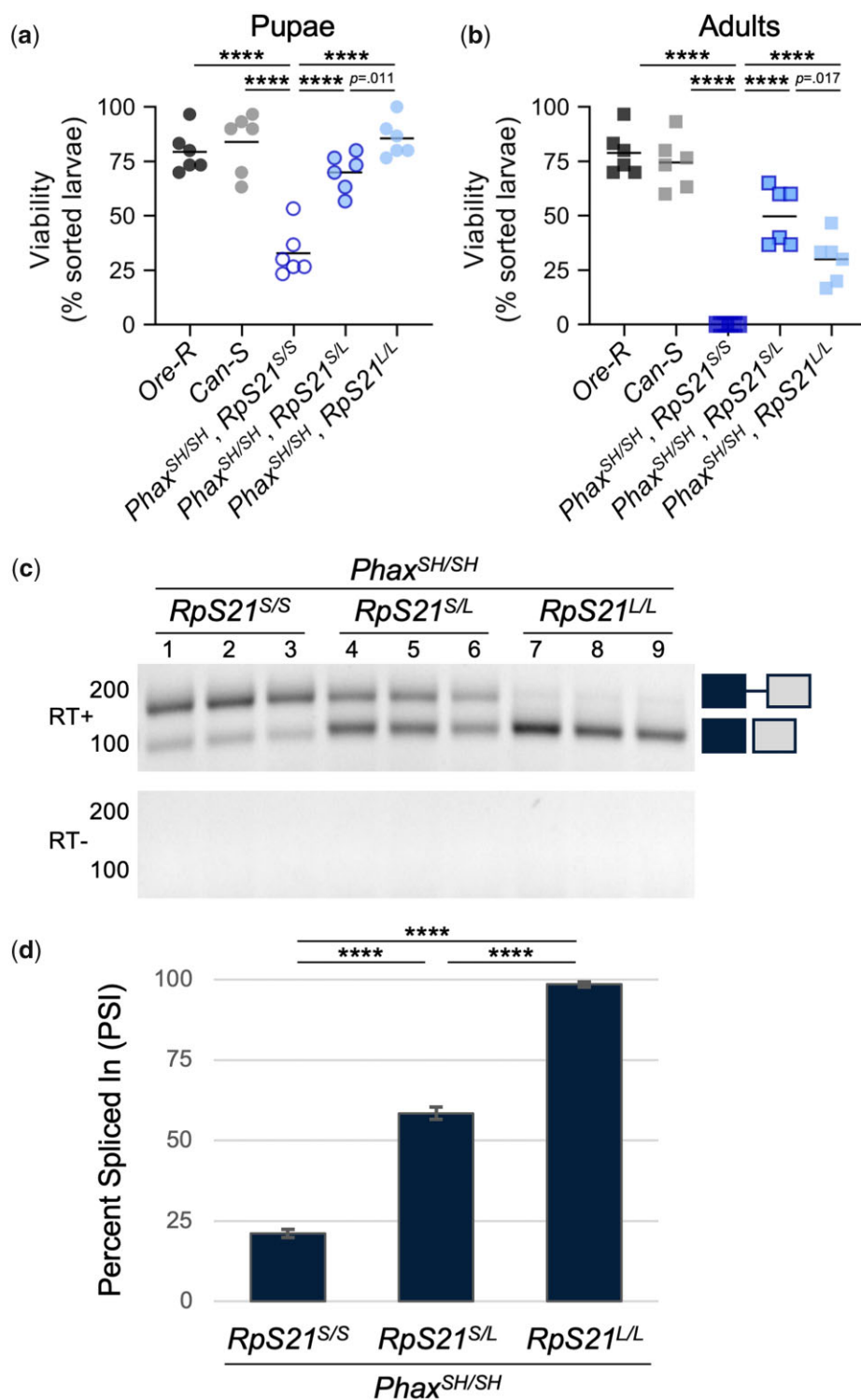


Fig. 6. Inverse correlation of Rps21 intron 3 retention with the viability of Phax^{SH/SH} mutants. Pupae (a) and adults (b) quantified as a percentage of sorted larvae from the genotypes indicated on the x-axis. Horizontal lines indicate the mean for each genotype. ****P < 0.0001. c) RT-PCR of Rps21 from the indicated genotypes. Images were inverted and contrast adjusted as indicated previously. d) Quantification of PSI of Rps21 transcripts from (c). ****P < 0.0001. Relative Rps21 intron 3 retention and percentage of spliced Rps21 transcripts in Phax^{SH/SH} mutants with the different Rps21 alleles.

terminal Rps21 coding exon and corresponding modulation of the carboxy terminus of the protein. The allele-specific Rps21 alternative splicing patterns uncovered here will aid the study of the alternative splicing control of Rps21 protein isoforms and their potential roles in ribosome biogenesis and homeostasis.

Data availability

All *Drosophila* stocks and plasmids are available upon request. The author affirms that all data necessary for confirming the conclusions of the article are present within the article, figures, and tables. RNA-seq analysis was performed on original fastq

files from the following GEO series accession numbers: Oregon-R, GSE49587 <https://www.ncbi.nlm.nih.gov/geo/query/acc.cgi?acc=GSE49587> and Phax^{SH/SH}, GSE81121 <https://www.ncbi.nlm.nih.gov/geo/query/acc.cgi?acc=GSE81121>.

Supplemental material is available at G3 online.

Acknowledgments

I gratefully acknowledge E.C. Garcia for sharing reagents, helpful discussions, and a critical reading of this article. I thank D.A. Harrison for helpful discussions, fly stocks, and fly food. I acknowledge A.G. Matera and B.C. Rymond for helpful discussions. I thank T.K. Rajendra for his insights into nuances of the Phax^{SH/SH} mutant line. I also thank K. Wolf and J. Jiang for the pellets of human cell lines used here. Fly stocks were obtained from the Bloomington *Drosophila* Stock Center (NIH P40OD018537), and *Drosophila* cell lines were obtained from the *Drosophila* Genomics Resource Center (NIH 2P40OD010949).

Funding

This work was supported by a grant to A.G. Matera from the National Institute of General Medical Sciences (R35-GM136435) and by a grant to ELG from the American Cancer Society (IRG-19-140-31).

Conflicts of interest

None declared.

Literature cited

- Akimov V, Barrio-Hernandez I, Hansen SVF, Hallenborg P, Pedersen A-K, Bekker-Jensen DB, Puglia M, Christensen SDK, Vanselow JT, Nielsen MM, et al. UbiSite approach for comprehensive mapping of lysine and N-terminal ubiquitination sites. *Nat Struct Mol Biol*. 2018;25(7):631–640.
- Aspesi A, Ellis SR. Rare ribosomopathies: insights into mechanisms of cancer. *Nat Rev Cancer*. 2019;19(4):228–238.
- Bernabò P, Tebaldi T, Groen EJM, Lane FM, Perenthaler E, Mattedi F, Newbery HJ, Zhou H, Zuccotti P, Potrich V, et al. *In vivo* translate profiling in Spinal Muscular Atrophy reveals a role for SMN protein in ribosome biology. *Cell Rep*. 2017;21(4):953–965.
- Black JJ, Johnson AW. Release of the ribosome biogenesis factor Bud23 from small subunit precursors in yeast. *RNA*. 2022;28(3):371–389.
- Bray NL, Pimentel H, Melsted P, Pachter L. Near-optimal probabilistic RNA-seq quantification. *Nat Biotechnol*. 2016;34(5):525–527.
- Cartegni L, Wang J, Zhu Z, Zhang MQ, Krainer AR. ESEfinder: a web resource to identify exonic splicing enhancers. *Nucleic Acids Res*. 2003;31(13):3568–3571.
- Carvalho GB, Ja WW, Benzer S. Non-lethal PCR genotyping of single *Drosophila*. *BioTechniques*. 2009;46(4):312–314.
- Chan YB, Miguel-Aliaga I, Franks C, Thomas N, Trülsch B, Sattelle DB, Davies KE, van den Heuvel M. Neuromuscular defects in a *Drosophila* survival motor neuron gene mutant. *Hum Mol Genet*. 2003;12(12):1367–1376.
- Chang HC-H, Dimlich DN, Yokokura T, Mukherjee A, Kankel MW, Sen A, Sridhar V, Fulga TA, Hart AC, Van Vactor D, et al. Modeling Spinal Muscular Atrophy in *Drosophila*. *PLoS One*. 2008;3(9):e3209.
- Cherbas P, Cherbas L, Lee SS, Nakanishi K. 26-[¹²⁵I]iodoponasterone A is a potent ecdysone and a sensitive radioligand for ecdysone receptors. *Proc Natl Acad Sci U S A*. 1988;85(7):2096–2100.
- Choudhary C, Kumar C, Gnäd F, Nielsen ML, Rehman M, Walther TC, Olsen JV, Mann M. Lysine acetylation targets protein complexes and co-regulates major cellular functions. *Science*. 2009;325(5942):834–840.
- Costa LD, Leblanc T, Mohandas N. Diamond-Blackfan anemia. *Blood*. 2020;136(11):1262–1273.
- Danecek P, Bonfield JK, Liddle J, Marshall J, Ohan V, Pollard MO, Whitwham A, Keane T, McCarthy SA, Davies RM, et al. Twelve years of SAMtools and BCFtools. *GigaScience*. 2021;10(2):giab008.
- Edgar R, Domrachev M, Lash AE. Gene Expression Omnibus: NCBI gene expression and hybridization array data repository. *Nucleic Acids Res*. 2002;30(1):207–210.
- Fernando C, Audibert A, Simon F, Tazi J, Juge F. A role for the serine/arginine-rich (SR) protein B52/SRSF6 in cell growth and Myc expression in *Drosophila*. *Genetics*. 2015;199(4):1201–1211.
- Garcia EL, Wen Y, Praveen K, Matera AG. Transcriptomic comparison of *Drosophila* snRNP biogenesis mutants reveals mutant-specific changes in pre-mRNA processing: implications for spinal muscular atrophy. *RNA*. 2016;22(8):1215–1227.
- Halder G, Johnson RL. Hippo signaling: growth control and beyond. *Development*. 2011;138(1):9–22.
- Hariharan IK. Organ size control: lessons from *Drosophila*. *Dev Cell*. 2015;34(3):255–265.
- Horos R, Ijspeert H, Pospisilova D, Sendtner R, Andrieu-Soler C, Taskesen E, Nieradka A, Cmejla R, Sendtner M, Touw IP, et al. Ribosomal deficiencies in Diamond-Blackfan anemia impair translation of transcripts essential for differentiation of murine and human erythroblasts. *Blood*. 2012;119(1):262–272.
- Hoskins RA, Carlson JW, Wan KH, Park S, Mendez I, Galle SE, Booth BW, Pfeiffer BD, George RA, Svirskas R, et al. The Release 6 reference sequence of the *Drosophila melanogaster* genome. *Genome Res*. 2015;25(3):445–458.
- Hu Y, Comjean A, Rodiger J, Liu Y, Gao Y, Chung V, Zirin J, Perrimon N, Mohr SE. FlyRNAi.org—the database of the *Drosophila* RNAi screening center and transgenic RNAi project: 2021 update. *Nucleic Acids Res*. 2020;49:gkaa936.
- Kahsai L, Millburn GH, Cook KR. Phenotypes associated with second chromosome P element insertions in *Drosophila melanogaster*. *G3 (Bethesda)*. 2016;6(8):2665–2670.
- Khajuria RK, Munschauer M, Ulirsch JC, Fiorini C, Ludwig LS, McFarland SK, Abdulhay NJ, Specht H, Keshishian H, Mani DR, et al. Ribosome levels selectively regulate translation and lineage commitment in human hematopoiesis. *Cell*. 2018;173(1):90–103.e19.
- Kim D, Paggi JM, Park C, Bennett C, Salzberg SL. Graph-based genome alignment and genotyping with HISAT2 and HISAT-genotype. *Nat Biotechnol*. 2019;37(8):907–915.
- Larkin A, Marygold SJ, Antonazzo G, Attrill H, Dos Santos G, Garapati PV, Goodman JL, Gramates LS, Millburn G, Strelets VB, et al.; FlyBase Consortium. FlyBase: updates to the *Drosophila melanogaster* knowledge base. *Nucleic Acids Res*. 2021;49(D1):D899–D907.
- Lefebvre S, Bürglen L, Reboullet S, Clermont O, Burret P, Viollet L, Benichou B, Cruaud C, Millasseau P, Zeviani M, et al. Identification and characterization of a spinal muscular atrophy-determining gene. *Cell*. 1995;80(1):155–165.
- Marygold SJ, Roote J, Reuter G, Lambertsson A, Ashburner M, Millburn GH, Harrison PM, Yu Z, Kenmochi N, Kaufman TC, et al. The ribosomal protein genes and Minute loci of *Drosophila melanogaster*. *Genome Biol*. 2007;8(10):R216.

- Matera AG, Wang Z. A day in the life of the spliceosome. *Nat Rev Mol Cell Biol.* 2014;15(2):108–121.
- Meng Z, Moroishi T, Guan K-L. Mechanisms of Hippo pathway regulation. *Genes Dev.* 2016;30(1):1–17.
- Mertins P, Mani DR, Ruggles KV, Gillette MA, Clauser KR, Wang P, Wang X, Qiao JW, Cao S, Petralia F, et al.; NCI CPTAC. Proteogenomics connects somatic mutations to signalling in breast cancer. *Nature.* 2016;534(7605):55–62.
- Mertins P, Qiao JW, Patel J, Udeshi ND, Clauser KR, Mani DR, Burgess MW, Gillette MA, Jaffe JD, Carr SA, et al. Integrated proteomic analysis of post-translational modifications by serial enrichment. *Nat Methods.* 2013;10(7):634–637.
- Mills EW, Green R. Ribosomopathies: there's strength in numbers. *Science.* 2017;358(6363):eaan2775.
- Munding EM, Shiue L, Katzman S, Donohue JP, Ares MJ. Competition between pre-mRNAs for the splicing machinery drives global regulation of splicing. *Mol Cell.* 2013;51(3):338–348.
- Narla A, Ebert BL. Ribosomopathies: human disorders of ribosome dysfunction. *Blood.* 2010;115(16):3196–3205.
- Oh S-W, Kingsley T, Shin H-h, Zheng Z, Chen H-W, Chen X, Wang H, Ruan P, Moody M, Hou SX, et al. A P-element insertion screen identified mutations in 455 novel essential genes in *Drosophila*. *Genetics.* 2003;163(1):195–201.
- Ohno M. Size matters in RNA export. *RNA Biol.* 2012;9(12):1413–1417.
- Ohno M, Segref A, Bachi A, Wilm M, Mattaj JW. PHAX, a mediator of U snRNA nuclear export whose activity is regulated by phosphorylation. *Cell.* 2000;101(2):187–198.
- Pimentel H, Bray NL, Puente S, Melsted P, Pachter L. Differential analysis of RNA-seq incorporating quantification uncertainty. *Nat Methods.* 2017;14(7):687–690.
- Pleiss JA, Whitworth GB, Bergkessel M, Guthrie C. Transcript specificity in yeast pre-mRNA splicing revealed by mutations in core spliceosomal components. *PLoS Biol.* 2007;5(4):e90.
- Rajendra TK, Gonsalvez GB, Walker MP, Shpargel KB, Salz HK, Matera AG. A *Drosophila melanogaster* model of Spinal Muscular Atrophy reveals a function for SMN in striated muscle. *J Cell Biol.* 2007;176(6):831–841.
- Robinson JT, Thorvaldsdóttir H, Wenger AM, Zehir A, Mesirov JP. Variant review with the Integrative Genomics Viewer. *Cancer Res.* 2017;77(21):e31–e34.
- Robinson JT, Thorvaldsdóttir H, Winckler W, Guttman M, Lander ES, Getz G, Mesirov JP. Integrative genomics viewer. *Nat Biotechnol.* 2011;29(1):24–26.
- Saltzman AL, Pan Q, Blencowe BJ. Regulation of alternative splicing by the core spliceosomal machinery. *Genes Dev.* 2011;25(4):373–384.
- Sanson B, White P, Vincent J-P. Uncoupling cadherin-based adhesion from wingless signalling in *Drosophila*. *Nature.* 1996;383(6601):627–630.
- Sato M, Kong CJ, Yoshida H, Nakamura T, Wada A, Shimoda C, Kaneda Y. Ribosomal proteins S0 and S21 are involved in the stability of 18S rRNA in fission yeast, *Schizosaccharomyces pombe*. *Biochem Biophys Res Commun.* 2003;311(4):942–947.
- Schenkel H, Hanke S, Lorenzo CD, Schmitt R, Mechler BM. P elements inserted in the vicinity of or within the *Drosophila* snRNP *SmD3* gene nested in the first intron of the *Ornithine Decarboxylase Antizyme* gene affect only the expression of *SmD3*. *Genetics.* 2002;161(2):763–772.
- Schneider I. Cell lines derived from late embryonic stages of *Drosophila melanogaster*. *J Embryol Exp Morphol.* 1972;27(2):353–365.
- Shi H, Hoffman BE, Lis JT. A specific RNA hairpin loop structure binds the RNA recognition motifs of the *Drosophila* SR protein B52. *Mol Cell Biol.* 1997;17(5):2649–2657.
- Srivastava D, Toledo M, Manchon L, Tazi J, Juge F. Modulation of Yorkie activity by alternative splicing is required for developmental stability. *EMBO J.* 2021;40(3):e104895.
- Stewart MJ, Denell R. Mutations in the *Drosophila* gene encoding ribosomal protein S6 cause tissue overgrowth. *Mol Cell Biol.* 1993;13(4):2524–2535.
- Tabb-Massey A, Caffrey JM, Logsdon P, Taylor S, Trent JO, Ellis SR. Ribosomal proteins Rps0 and Rps21 of *Saccharomyces cerevisiae* have overlapping functions in the maturation of the 3' end of 18S rRNA. *Nucleic Acids Res.* 2003;31(23):6798–6805.
- Talkish J, Igel H, Perriman RJ, Shiue L, Katzman S, Munding EM, Shelansky R, Donohue JP, Ares M. Rapidly evolving protointrons in *Saccharomyces* genomes revealed by a hungry spliceosome. *PLoS Genet.* 2019;15(8):e1008249.
- Török I, Herrmann-Horle D, Kiss I, Tick G, Speer G, Schmitt R, Mechler BM. Down-regulation of RpS21, a putative translation initiation factor interacting with P40, produces viable *Minute* imago and larval lethality with overgrown hematopoietic organs and imaginal discs. *Mol Cell Biol.* 1999;19(3):2308–2321.
- Wada Y, Ohsawa S, Igaki T. Yorkie ensures robust tissue growth in *Drosophila* ribosomal protein mutants. *Development.* 2021;148(14):dev198705.
- Watson KL, Konrad KD, Woods DF, Bryant PJ. *Drosophila* homolog of the human S6 ribosomal protein is required for tumor suppression in the hematopoietic system. *Proc Natl Acad Sci U S A.* 1992;89(23):11302–11306.
- Yu F-X, Zhao B, Guan K-L. Hippo pathway in organ size control, tissue homeostasis, and cancer. *Cell.* 2015;163(4):811–828.

Communicating editor: H. Salz